Optical Materials 133 (2022) 112964

Contents lists available at ScienceDirect

Optical Materials

journal homepage: www.elsevier.com/locate/optmat

Research Article

Structural, optical, dielectric and photovoltaic properties of Sn doped CdS films prepared with green synthesis route

Rida Jaffar [a], M.I. Khan [a,*], Ghulam M. Mustafa [b], S.S. Ali [c], Lamia Ben Farhat [d,e], Zainab Mufarreh Elqahtani [f], Norah Alwadai [f]

[a] Department of Physics, The University of Lahore, Lahore, 53700, Pakistan
[b] Department of Physics, Division of Science and Technology, University of Education, Lahore, Pakistan
[c] School of Physical Sciences, University of the Punjab, Pakistan
[d] Department of Chemistry College of Sciences, King Khalid University, P.O. Box, 9004, Abha, Saudi Arabia
[e] Laboratoire des Mat'eriaux et de l'environnement pour le D'eveloppement Durable LR18ES10, 9 Avenue Dr. Zoheir Sai, 1006, Tunis, Tunisia
[f] Department of Physics, College of Sciences, Princess Nourah bint Abdulrahman University, P.O. Box 84428, Riyadh, 11671, Saudi Arabia

ARTICLE INFO

Keywords:
Photo-absorber
Green synthesis
Optical parameters
Solar cells

ABSTRACT

Energy harvesting from renewable energy sources is one of the burning topics in today's research community. Solar cells are emerging as a potential candidate to harvest solar energy into electrical one. Here, we tested a series of pure and Sn-doped CdS as photoabsorbers in solar cells prepared by the sol-gel technique via the green synthesis route. The formation of a hexagonal wurtzite crystal structure of pure and Sn-doped CdS is confirmed using X-ray diffraction analysis. Doping of Sn caused a slight change in lattice parameters, crystallite size, d-spacing, and dislocation line density. UV–vis measurement revealed the direct bandgap nature of the material with bandgap value of 2.50 eV which reduced the 2.20 eV upon 3% Sn doping. Optical parameters, including extinction coefficient and refractive index, are measured. The film prepared with 3% of Sn doping has a high refractive index, i.e., 2.56. In addition, the imaginary and real parts of the dielectric constant are measured in the frequency range of 20Hz to 20 MHz, which exposed the presence of different relaxation phenomena in this composition. The solar cell prepared with 3% of Sn doping has a high value of current density (3.57 mA-cm^{-2}), open circuit voltage (0.49 V), fill factor (0.654) and efficiency (1.14%). This solar cell is a stable cell due to the absence of liquid corrosion like in dye-sensitized solar cells.

1. Introduction

Earth abundance is regarded as a key condition for photovoltaic (PV) absorbers that can not only meet but also maintain the terawatt energy output target [1]. The two most emerging thin-film technologies, achieving this aim (i.e., CdTe [2] and Cu(In,Ga)Se_2 [3] are concern due to supply and cost issues of Ga, In, and Te [4]. In some cases, attempts are made to substitute tin and zinc for the expensive and scarce indium in Cu(In, Ga)Se_2 (CIGS), resulting in $Cu_2(ZnSn)(SSe)_4$ (CZTS) [5]. However, theoretical analyses have shown numerous significant difficulties with CZTS [6], the majority of which stem from the multi-valence of Sn and the material's restricted stability range [7,8]. As a result, simple binary Earth-abundant absorbers like CdS [9], FeS_2 [9], and $Cu_{2-x}S$ [10] have lately piqued the PV community's interest [11].

The practical uses of II-VI nanomaterials in a range of optoelectronics, such as highly efficient thin film transistors, electron-beam pump lasers, light-emitting diodes [12], and electroluminescent devices [13–15] are now of significant interest. Due to their unique features, semiconductors materials are used to make the majority of PV cells. The semiconductors material absorbs photons at a certain wavelength and produces free electrons, which provide an electric current [16]. CdS has emerged as a promising material for a variety of photovoltaic applications. The thermal and optical characteristics of solar cells have received special attention in order to increase their performance. The absorbance spectrum may generally be measured using the traditional transmit intensity method, but samples must be suitably thin and have an excellent quality surface as a result of pretreatments [17].

However, the undoped CdS films have a high electrical resistance at room temperature [18], limiting their utility in solar cells. The dark resistivity of undoped CdS films should be decreased from 10^7–10^9 Ωcm

* Corresponding author.
E-mail address: muhammad.iftikhar@phys.uol.edu.pk (M.I. Khan).

https://doi.org/10.1016/j.optmat.2022.112964
Received 26 June 2022; Received in revised form 14 August 2022; Accepted 1 September 2022
Available online 18 September 2022
0925-3467/© 2022 Elsevier B.V. All rights reserved.

to at most 10 Ωcm to make them useable in optoelectronic applications [19]. Although it is highly dependent on its preparation procedures, thin films cannot be prepared to the required standards. Some post-deposition techniques, on the other hand, have been observed to lower electrical resistivity [20]. An external atom with fewer or more valence electrons than the pristine atom is another effective technique to get the desired features. Impurities with fewer electrons act as acceptors, resulting in p-type conductivity, whereas those with more electrons function as donors, resulting in n-type conductivity. Lee et al. [21] investigated the electro - optic characteristics of chemical bath-deposited B-doped CdS films. Sebastian [22] also reported in bath deposited p-type Cu–CdS thin films. Megahid and his colleagues [23] used electron beam evaporation to create In doped CdS thin films with n-type conductivity [24].

Sn is a good electron-efficient material and it reacts with sulphur to form a promising semiconductor material for photovoltaic applications. The recombination of electron and hole in CdS-based solar cells is a major issue which affects the efficiency of solar cells. Sn reduces the recombination rate; therefore, it increases the efficiency and stability of solar cells. Therefore, Sn has been doped in CdS film to improve its electrical and photovoltaic properties.

In this study, we have used Sn as a dopant material to improve the stability and photovoltaic properties of CdS-based solar cells. Sn has reduced the E_g and recombination rate of CdS. This will increase the cell's efficiency. There is no study related to Sn-doped CdS-based solar cells in the literature.

2. Experimentation

Aloe vera gel extract was used in the hydrothermal preparation of Cd–SnS materials. Aloe vera gel quickly reduced the metals by reacting with them. SnS content was created as a result in about 8 h. The synthesis process took 14–18 h if just water was utilized. For making cadmium sulfide, take the amount of 4 ml ethylene glycol, $CdNO_3$ (3.0847) g\mole and thiourea (0.7612) g\mole mix in 100 ml of green extract water, stir for 1 h at 410 rpm and name it as solution 1. Take another breaker, add 100 ml of water, and mix 12 g NaOH. The solution of NaOH will be continuously added by using the pipette dropwise into the solution 1 until the pH reaches 7. Similarly, three more solutions were prepared. In these solutions (1, 2, and 3 wt%) of $SnCl_2$ were added before adding the NaOH. After that, the NaOH was introduced dropwise and continuously stirred until the formation of gel took place. These remedies lasted for 22 h. Four slides of FTO-glass substrates were rinsed with di-ionized water, ethanol, and ultrasonically. Films of (0, 1, 2, and 3%) Sn–CdS were prepared by adding four drops of solutions on FTO-glass substrates having 2000 rev/min. these films were heated at 100 °C for 10 min. After those four films of (0, 1, 2, and 3%) Sn–CdS were prepared on FTO-glass substrates.

An X'Pert Philips diffractometer (XRD) was used to assess structural properties (XRD). A 3700 UV-VIS-NIR SolidSpec Shimadzu spectrophotometer was used to analyze the optical properties. A precise impedance analyzer was used to measure the dielectric characteristics.

2.1. Solar cells fabrication

The soluble Sn–CdS solution (0, 1, 2, and 3%) were deposited on TiO_2/FTO/glass substrates using a spin coater with a speed of 2000 rev/min in order to construct solar cells. The same method used in our previously published article was adopted to deposit TiO_2 film on FTO/glass substrates [25]. A P3HT polymer layer that serves as a hole transport layer was applied above all of the films using a spin coater with a 6000 rev/min rotating speed. A gold (Au) contact was created above that. Glass/FTO/TiO_2/CdS/P3HT/Au made up the cell's new shape.

A surface profilometer was used to measure the film thickness. The thickness of TiO_2, CdS, and P3HT are 300 nm, 450 nm, and 200 nm, respectively. A solar simulator (Kiethley 2400, 100 mW/cm^2 irradiation, recorded on the AM 1.5 spectra) was used to characterize solar cells. Fig. 1 depicts the layer-by-layer deposition in steps.

3. Results and discussion

3.1. Structural analysis

Fig. 2 (a) shows the XRD patterns of pure and Sn-doped CdS, which are used to calculate the interplanar spacing, size of crystallite, lattice parameters, and dislocation line density. The diffracted peaks that appeared at 2θ values of 28.292°, 36.152°, 43.803°, and 47.807° were indexed as (101), (102), (110), and (103). These peaks were matched with PDF # 65–3414, which assured the formation of a wurtzite hexagonal phase of CdS [26]. When 1%, 2% and 3% Sn is doped in CdS it did not introduce any new phase therefore, no new peak is appeared. However, there is a tiny movement in the peaks towards larger 2 values, which suggests that the volume of the unit cell has increased. Overall, it has been found that peak intensity increases as Sn concentration does, which indicates that the doping of Sn facilitates the crystal growth.

The full width at half maximum (FWHM) (β) for the largest peak's intensity is noted and used to calculate the size of crystallite using the Scherrer formula [27]:

$$D = \frac{0.9\lambda}{\beta COS\theta} \tag{1}$$

where λ and θ are wavelength and Bragg's angle, respectively. The calculation of D leads to determining the dislocation line density (δ). The δ is linked with the D as:

$$\delta = \frac{1}{D^2} \tag{2}$$

The small value of δ confirms that Sn doping may produce CdS nanostructures with low defects. Thus, in present case, a smaller value of δ reflects the better quality of thin films. The dislocation line density relates to the defects inside the crystalline materials, while crystallite size is related to the length of the grains. For pure CdS, the value of crystallite size is noticed as 14.8 nm and the value of dislocation line density is 0.45 × 10^{16} m^{-2} as shown in Fig. 2(b). The 'D' increases to 15.7 nm when doped with 1% Sn, but δ decreases to 0.40 × 10^{16} m^{-2}. This increase in crystallite size is attributed to the Sn doping and it particularly occurs near the grain limits. For 2% and 3% doping of Sn, these values are noted as 18.9 nm and 0.27 × 10^{16} m^{-2} and 25.2 nm and 0.15 × 10^{16} m^{-2}, respectively. This increase in D and decrease in δ is good for the photoelectrode functionality of solar cells [28]. The measured values of δ and D are shown in Table 1.

The change of d-spacing with doping concentration is shown in Fig. 2 (c). The interplanar spacing (d) is another key factor to estimate the size of the crystal. The d is calculated using Bragg's diffraction condition [29]:

$$d = \frac{n\lambda}{2\sin\theta} \tag{3}$$

The value of d-spacing for pure and 1% Sn-doped CdS is noticed as 3.150 Å, which increased to 3.160 Å when 2% Sn is doped. 1% doping did not change the d-spacing because all Sn took the interstitial positions however, when doping concentration is increase there are fewer interstitial sites available and doping started affecting the d-spacing. However, 3% doping again caused a decrease in d-spacing. This reduction in d-spacing can be brought on by the unit cell volume contracting. All these noted values are very similar to the standard values. Fig. 2(d) shows the variation of lattice parameters of pure and Sn-doped CdS. The lattice parameters of the hexagonal wurtzite unit cell can be calculated using the following relation [30].

$$\frac{1}{d^2} = \frac{4}{3}\left(\frac{h^2 + hk + k^2}{a^2}\right) + \frac{l^2}{c^2} \tag{4}$$

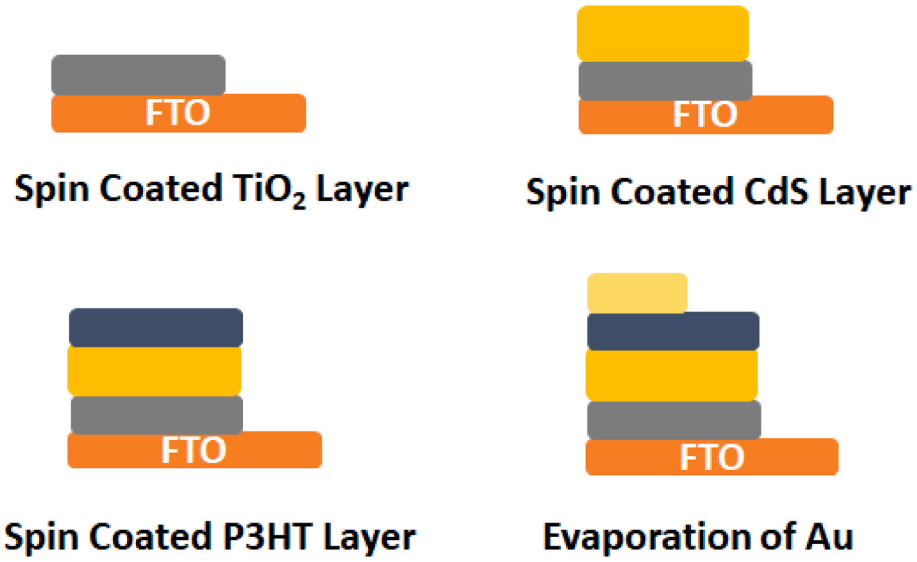

Fig. 1. Step wise deposition of different layers.

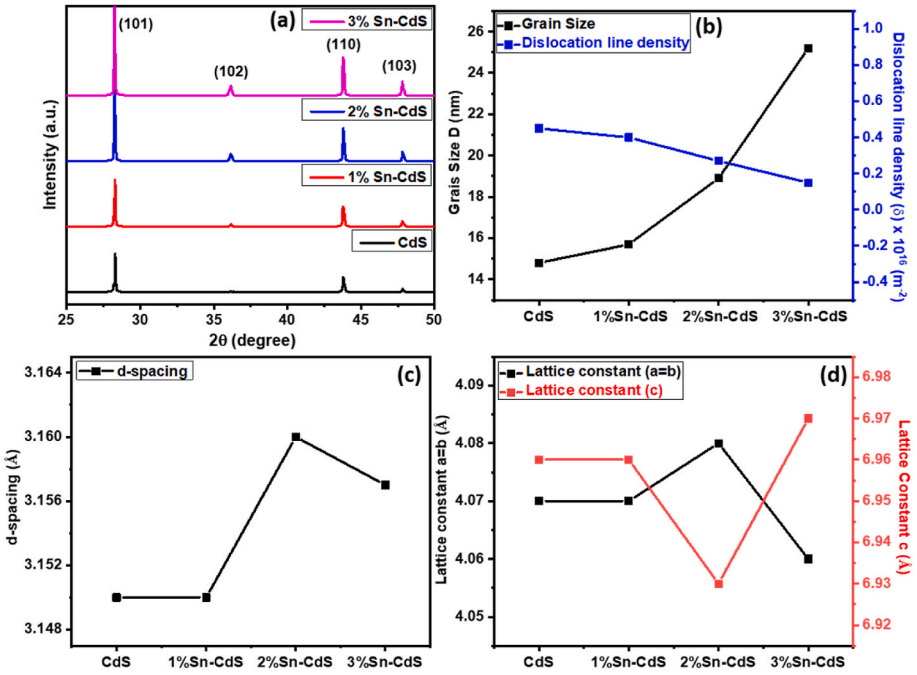

Fig. 2. (a) XRD patterns for all the synthesized Sn–CdS samples, (b) variation of δ and D, (c) d-spacing and (d) variation of lattice constants of pure and Sn doped CdS.

Table 1
Calculated values for δ, D, and d-spacing for all compositions.

Composition	Dislocation Line Density (δ)	Grain Size D(nm)	d-spacing (Å)
Pure CdS	0.45×10^{16}	14.8	3.15
1% Sn–CdS	0.40×10^{16}	15.7	3.15
2% Sn–CdS	0.27×10^{16}	18.9	3.16
3% Sn–CdS	0.15×10^{16}	25.2	3.18

Table 2
Lattice parameters values and volume of unit cell.

Composition	Lattice Parameter (Å)	Unit Cell Volume $(Å)^3$
Pure CdS	a = b = 4.07, c = 6.00	99.8
1% Sn–CdS	a = b = 4.07, c = 6.96	99.8
2% Sn–CdS	a = b = 4.08, c = 6.93	99.9
3% Sn–CdS	a = b = 4.06, c = 6.97	99.5

Here, *a* and *c* being lattice parameters, (*hkl*) and d are miller indices, and interplanar spacing, respectively. The value of a and c remains almost constant for pure and 1% doped Sn. The 'a' parameter increases while the c decreases in a 2% and reciprocal happened for 3% Sn–CdS thin film. The reason for this is that Sn atoms bend the crystallites of the Sn–CdS thin film, causing compressive strain and changing the lattice parameters.

3.2. UV results

UV–Vis spectrophotometer is a powerful technique to study the optical characteristics of undoped and Sn–CdS thin films, such as extinc-

tion coefficients (k), dielectric constants, band gap energy (E_g), and refractive index (n). To compute E_g of pure and Sn–CdS, the tauc plot is drawn as shown in Fig. 3 [31].

$$(\alpha h\upsilon)^2 = B\left(h\upsilon - E_g\right) \tag{5}$$

The Tauc plot is a graph between $(\alpha h\nu)^n$ and $h\nu$ where h, α, and ν are the Planck's constant, absorption coefficient, and incidence photon frequency. Constant n is determined by the kind of transition. For direct band transition, its value is 2, and for indirect bandgap it is 1/2 [28]. For the forbidden region, its value becomes 1/3 and 2/3 for direct and indirect bandgap materials. These tauc plots expose the direct band gap nature of these compositions. The value of bandgap (E_g) is determined by drawing a tangent to the line somehow parallel to the y-axis. The E_g value is provided at the location where this line crosses the x-axis [8]. The E_g value of pure CdS film is 2.50 eV. Doping a CdS thin film with 1% Sn reduced the E_g to 2.44 eV. This reduction in bandgap is due to the fact that Sn doping introduced new energy levels in the bandgap [28]. When 2% and 3% Sn are doped into the CdS, E_g is further reduced to 2.34 and 2.20 eV, respectively. This reduction in E_g value is also linked with the increase in crystallite size. Therefore, we can say that doping of Sn in CdS introduces more energy levels inside the E_g of the CdS film as a result, E_g shift to a lower value. This fact can also be linked with the quantum confinement phenomenon according to the Brus equation. This equation states that the E_g increases as the size of the nanoparticle decreases, and vice versa [32]. At 4% doping, the E_g is increased. The high amount of Sn is spread on the surface due to the limited number of vacant sites in CdS. Therefore, the band gap has increased.

3.3. Refractive index

Refractive index (n) is one of the key factors to map the path of light particularly when it transmit from one medium to other medium and thus provide help to determine the relative speed of light in different media. The 'n' and 'E_g' are related as [33]:

$$n^4 E_g = 95\ eV \tag{6}$$

The band gap energy and optical refractive index are E_g and n, respectively. The reflective index is increased by doping Sn into the CdS films, as shown in Fig. 4 [34]. (0%, 1%, 2%, 3%, and 4%) Sn–CdS films have refractive indices of 2.512, 2.534, 2.571, 2.626, and 2.594, respectively. The refractive index values of all the CdS films are very similar, with little change. Similarly, the refractive index has another expression [33].

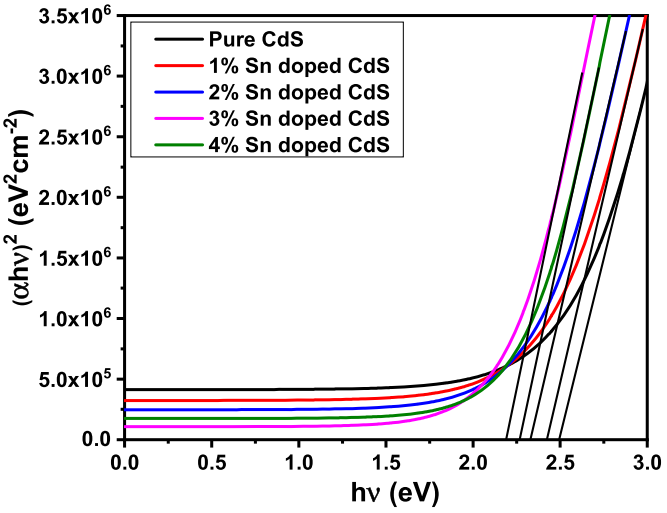

Fig. 3. Bandgap calculation of pure and Sn-doped CdS.

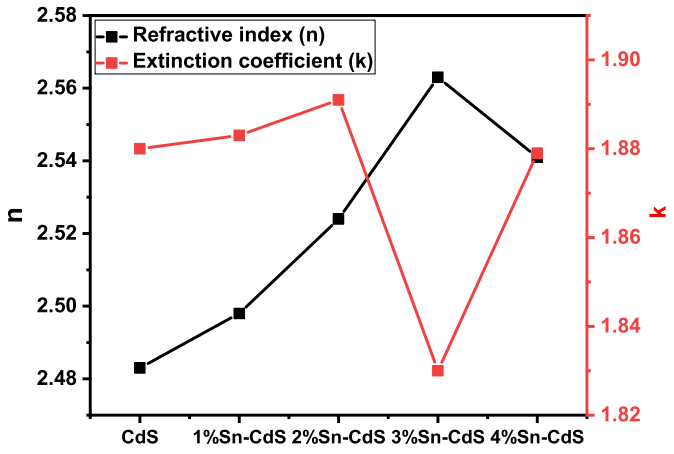

Fig. 4. k and n of pure and Sn doped CdS.

$$n = \sqrt{1 + \left(\frac{A}{E_g + B}\right)^2} \tag{7}$$

where B (3.4 eV) and A (13.6 eV) are constants [35]. It is observed that the reflective index increases by Sn–CdS (0%–3%). It is supposed that the increasing refractive indexes overcome by CdS films due to Sn doping make them suitable for use as anti-reflection coatings and will increase the efficiency of solar cells [36].

3.4. Extinction coefficient (k)

The determination of the rate of decrease of transferred light via dispersion and absorption in any medium is known as the extinction coefficient. The formula below is used to determine the 'k' of pure and Sn–CdS films [37,38]:

$$k = \frac{n}{\Delta\chi^{*r}} \tag{8}$$

Here k and $\gamma = -0.32$ are constants, (n) refractive index and ($\Delta\chi^*$) electro negativity difference.

The variation of the extinction coefficient with the doping of Sn is presented in Fig. 4. The extinction coefficients of (0%, 1%, 2%, 3%, and 4%) is noticed as 1.880, 1.883, 1.891, 1.830, and 1.879, respectively. From Fig. 4, it can be seen that with the increase of Sn doping concentration up to 2%, 3%, the values of extinction coefficient decrease to 1.83 and the value of reflective index increases to 2.56. When 4% Sn doping concentration is reached, the value of the extinction coefficient is increased to 1.88 and the value of the reflective index is decreased to 2.54. The change in value of 'k' and 'n' refers to the chemical characteristics of CdS film altering with doping [39]. The presence of free electrons in strongly doped CdS leads to greater absorption of incoming visible light, which enhances the photovoltaic performance of SnS-based solar cells [40].

3.5. Dielectric constants

Dielectric constant is another optical parameter used to investigate the optical behavior of the material. It is a complex quantity and related directly with the k and n [38].

$$\varepsilon = \varepsilon' + \varepsilon'' \tag{9}$$

The real part of the dielectric constant measures how much light is absorbed by the material for later use, and the imaginary part quantifies the proportion of light that is lost by dispersion or absorption. The absorption of light occurs due to the polarization of atoms and molecules present in the material. However, energy loss is quantified by the ratio of

ε' and ε'' [41]. The relation of dielectric constant with the refractive index and extinction coefficient are given below:

$$\varepsilon' = n^2 - k^2 \tag{10}$$

$$\varepsilon'' = 2nk \tag{11}$$

The variation in the dielectric constants is shown in Fig. 5. The dielectric constant of pure and Sn-doped (0%, 1%, 2%, 3%, and 4%) thin films is 2.630, 2.691, 2.793, 3.217, and 2.923, respectively. It is observed that with an increase of Sn concentration to 1% and 2%, the value of imaginary and real dielectric constants (ε'', ε') is increased. When Sn concentration is increased to 3%, the ε'' is decreased and the ε' is increased. When 4% Sn is doped into the CdS, its ε'' is increased and its ε' is decreased. Photon energy is used by both ε'' and ε' parts. For our films, the imaginary portion (ε'') is greater in value than the real portion (ε').

The frequency-dependent dielectric behavior of these compositions is shown in Fig. 6. Fig. 6 (a) shows the variation of the real part of the dielectric constant (ε') against the frequency (Logf). From this diagram, it has been observed that in the low frequency region, the value of ε' is maximum which exponentially decreases with frequency (f) and became almost independent on frequency in the high region of frequency [42]. This type of behavior is understood on the basis of interfacial polarization caused by the accumulation of charges at the interfaces [43]. In the low frequency region, the charges at the interface get maximum time to polarize and give a maximum value of ε'. As the frequency is increased, the value of ε' is decreased, which is attributed to the decrease in relaxation time of charges at the interface. Fig. 6(b) shows the changing of loss tangent (tanδ) with frequency. The value of tanδ is also high in the low frequency zone, which decreases as frequency increased. The peaks that appear in these graphs, particularly for 2% and 3% Sn doped-CdS, are relaxation peaks and thus show the presence of relaxation phenomena present in these compositions [44]. It is obvious from these graphs that peaks are shifted towards high frequency value which indicates the decrease in relaxation time.

Fig. 7 (a) shows the variation of real part of impedance (Z′) with frequency (Logf). This graph shows identical behavior as that of ε' i.e., maximum value in the low frequency range. The value of Z′ quantifies interface resistance in the multilayer system. The interface region is frequency sensitive and shows different behavior in different frequency regimes. In the low frequency region, it offers more resistance. However, as the frequency increases, the resistivity of the interface diminishes and becomes almost constant in the high frequency zone.

The graph between imaginary (Z″) and real (Z′) part of impedance is called Nyquist plot and is more reliable approach to distinguish the behavior of different electroactive regions in different frequency domains [45].

The Nyquist plot for all these compositions is shown in Fig. 7 (b). For all compositions, it is semicircular in shape. For pure and 1% Sn doping, there are two overlapped semicircles, while for 2% and 3% Sn doping, only one semicircle is achieved. The diameter of these semicircles gives rise to the value of interface resistance. It has been observed that doping of Sn causes an increase in the resistance of CdS. This is because of the fact that Sn is more electropositive [46]. As its concentration increases, it provides more electrons which accumulate at the interface and give rise to a high value of impedance.

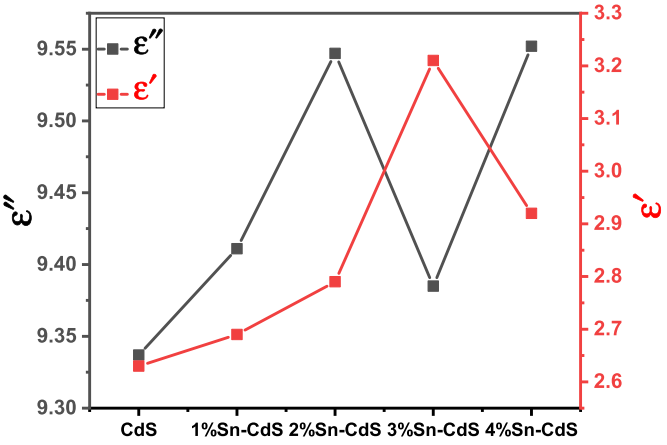

Fig. 5. Imaginary and real parts of dielectric constant of pure and Sn doped CdS.

3.6. J-V measurement

To estimate the photoconversion efficiency of pure and Sn-doped CdS, fill factor (FF), current density (J_{SC}), efficiency (η), and open circuit voltage (V_{OC}) are measured. Fig. 8 shows the J-V curve of different solar cells. The value of J_{SC}, depends on initially generated photogenerated carriers, injection efficiency, and recombination rate [47]. The recombination rate is governed by the oxidized dye in the electrolyte. The value of open circuit voltage is determined by:

$$V_{OC} = |E_F - E_{redox}| \tag{12}$$

Here, the electrolyte's energy level is called E_{redox}, while the fermi level is known as E_F. If V_{OC} is large, it means there is a large difference between fermi and redox level [48]. The values of FF and η are computed using the following relations [49]:

$$FF = \frac{I_{max} \times V_{max}}{J_{SC} \times V_{OC}} \tag{13}$$

$$\eta = \frac{FF \times V_{OC} \times J_{SC}}{P_{in}} \tag{14}$$

Here, I_{max} and V_{max} are the maximum values of current and voltage, respectively (see Table 2). For pure CdS, the value of V_{oc}, J_{sc}, η, and FF are noticed to be 0.489 V, 2.68 mA-cm^{-2}, 0.482 and 0.63%, respectively. When 1% Sn is doped in CdS, the value of J_{SC} increased from 2.68 to 3.00 mA-cm^{-2}, V_{OC} remained constant (0.489 V), FF increased from 0.482 to 0.532, which resulted in an increase in efficiency from 0.63 to 0.78. The increase in J_{SC} speaks about the enhancement of injection efficiency of the cell with the reduction of the recombination rate. Electron transfer efficiency, light scattering, and efficiency of adsorption of dye all have an impact on J_{sc} [50–52].When more electrons will transfer then recombination rate will reduce. Similarly, the increased value of η convinces that Sn doping improved the electronic features of pure CdS. When the doping concentration of Sn is increased to 2% and 3%, the percentage efficiency increases to 0.95 and 1.14, which represents the reduction in recombination rate of hole-electron pairs [53]. However, when the doping amount is increased to 4%, the efficiency is slightly decreased. To enhance the η of photoanode of DSSCs, the value of J_{sc} and V_{oc} need to be increased. Since the quantum efficiency of DSSCs depends upon the absorption capacity of sensitizer dye, which is one of the possible causes of the increase in efficiency of DSSCs in the present case. When the Sn doping amount is increased to 4%, the values of Jsc and FF are decreased, which is due to the high recombination rate of hole-electron pairs caused by the overdoping of Sn. This decrease in efficiency is also attributed to the creation of an additional accepter level above the fermi level of CdS. 3% Sn-doped CdS is an optimized composition because it gives the maximum value of power conversion efficiency [54]. The measured values of all these factors are summarized in Table 3.

4. Conclusion

In this study, we employed the sol-gel method via the green synthesis route to prepare undoped and Sn-doped CdS films. According to XRD,

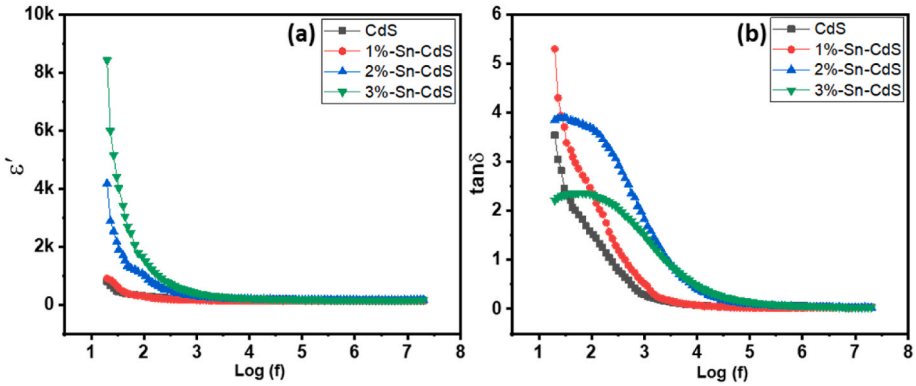

Fig. 6. Frequency dependent (a) Real and (b) imaginary part of dielectric constant of pure and Sn doped CdS.

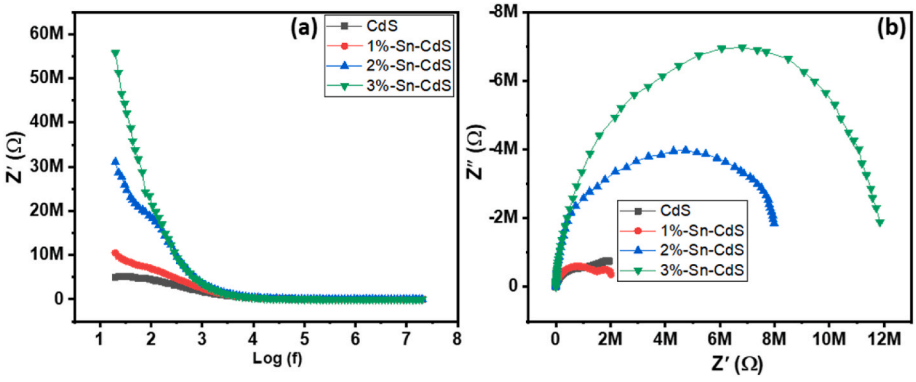

Fig. 7. Frequency dependent (a) Real part of impedance (b) Nyquist plot pure and Sn doped CdS.

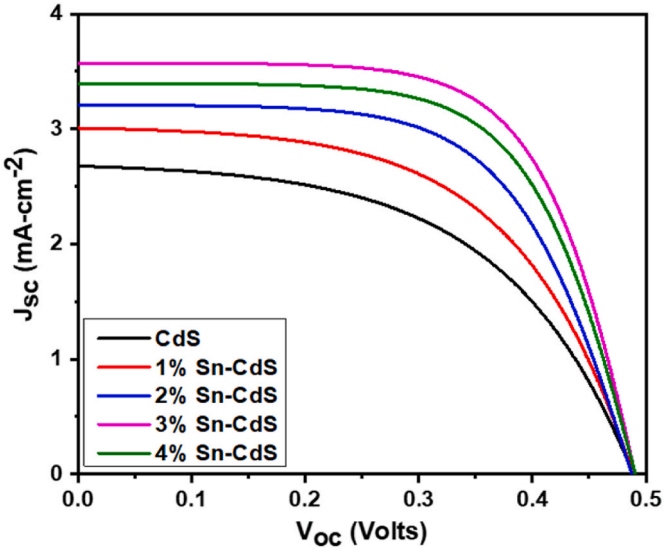

Fig. 8. JV curves of pure and Sn doped CdS.

Table 3
V_{oc}, J_{sc}, η, and FF of pure and Sn–CdS solar cells.

Samples	J_{sc} (mA-cm^{-2})	V_{oc} (V)	FF	η%
CdS	2.68	0.489	0.482	0.63
1% Sn–CdS	3.00	0.489	0.532	0.78
2% Sn–CdS	3.21	0.487	0.609	0.96
3% Sn–CdS	3.57	0.49	0.654	1.14
4% Sn–CdS	3.39	0.49	0.639	1.06

the films were made of hexagonal wurtzite crystals. The Sn doping in the CdS film was 3%, and the grain size was large (25.2 nm). This film also includes d-spacing (3.15 Å), dislocation line density (0.15×10^{16} m^{-2}), and lattice parameters (a = b = 4.06 Å, c = 6.9 Å). By using UV–Vis spectroscopy, the dielectric constants, refractive index, bandgap energy, and extinction coefficients are calculated for pure and Sn-doped CdS films. The formation of increased energy levels inside the CdS bandgap resulted in a reduction in E_g (2.20 eV) for 3% Sn doped CdS film. The highest refractive index was observed in the CdS film produced with 3% Sn doping (2.54). Because of its high dispersion, this material is suitable for solar cells. According to the J-V curve, the 3% Sn–CdS-based solar cell has the highest efficiency (1.14%) of all produced cells due to its large J_{sc} (3.57 mA/cm^{-2}), V_{oc} (0.49V), and fill factor (0.654). Due to Sn doping, the electron transport rate has improved and charge recombination has been retarded at the CdS-dye interface, resulting in increased efficiency.

CRediT authorship contribution statement

Rida Jaffar: Data curation, Writing – original draft. **M.I. Khan:** Data curation, Formal analysis, Writing – original draft. **Ghulam M. Mustafa:** Writing – original draft. **S.S. Ali:** Methodology. **Lamia Ben Farhat:** Funding acquisition, Methodology. **Zainab Mufarreh Elqahtani:** Funding acquisition, Investigation, Project administration. **Norah Alwadai:** Investigation, Resources, Supervision.

Declaration of competing interest

The authors declare that they have no known competing financial interests or personal relationships that could have appeared to influence the work reported in this paper.

Data availability

No data was used for the research described in the article.

Acknowledgement

The authors express their gratitude to Princess Nourah bint Abdulrahman University Researchers Supporting Project (Grant No. PNURSP2022R124), Princess Nourah bint Abdulrahman University, Riyadh, Saudi Arabia. The authors extend their appreciation to the Deanship of Scientific Research at King Khalid University, Saudi Arabia for funding this work through Research Groups Program under grant number R.G.P.2:187/43.

References

[1] C. Wadia, A.P. Alivisatos, D.M. Kammen, Materials availability expands the opportunity for large-scale photovoltaics deployment, Environ. Sci. Technol. 43 (6) (2009) 2072–2077.
[2] J. Britt, C. Ferekides, Thin-film CdS/CdTe solar cell with 15.8% efficiency, Appl. Phys. Lett. 62 (22) (1993) 2851–2852.
[3] I. Repins, et al., 19· 9%-efficient ZnO/CdS/CuInGaSe2 solar cell with 81· 2% fill factor, Prog. Photovoltaics Res. Appl. 16 (3) (2008) 235–239.
[4] D. Bauer, et al., Critical Materials Strategy, US Department of Energy, 2011. Google Scholar There is no corresponding record for this reference.
[5] H. Katagiri, Cu2ZnSnS4 thin film solar cells, Thin Solid Films 480 (2005) 426–432.
[6] K. Biswas, S. Lany, A. Zunger, The electronic consequences of multivalent elements in inorganic solar absorbers: multivalency of Sn in Cu 2 ZnSnS 4, Appl. Phys. Lett. 96 (20) (2010), 201902.
[7] A. Redinger, et al., The consequences of kesterite equilibria for efficient solar cells, J. Am. Chem. Soc. 133 (10) (2011) 3320–3323.
[8] T. Tanaka, et al., Influence of composition ratio on properties of Cu2ZnSnS4 thin films fabricated by co-evaporation, Thin Solid Films 518 (21) (2010) S29–S33.
[9] P. Sinsermsuksakul, et al., Atomic layer deposition of tin monosulfide thin films, Adv. Energy Mater. 1 (6) (2011) 1116–1125.
[10] A. Ashour, The physical characteristics of Cu~ 2S/CdS thin-film solar cell, J. Optoelectron. Adv. Mater. 8 (4) (2006) 1447.
[11] J. Vidal, et al., Band-structure, optical properties, and defect physics of the photovoltaic semiconductor SnS, Appl. Phys. Lett. 100 (3) (2012), 032104.
[12] P. Khanna, N. Singh, Light emitting CdS quantum dots in PMMA: synthesis and optical studies, J. Lumin. 127 (2) (2007) 474–482.
[13] D. Patidar, et al., Energy band gap and conductivity measurement of CdSe thin films, Chalcogenide Lett. 5 (2) (2008) 21–25.
[14] P. Guyot-Sionnest, Colloidal quantum dots, Compt. Rendus Phys. 9 (8) (2008) 777–787.
[15] T. El-Brolossy, et al., Photoacoustic characterization of optical and thermal properties of CdSe quantum dots, Eur. Phys. J. Spec. Top. 153 (1) (2008) 365–368.
[16] G. Mnasri, et al., Characterization and study of CdS quantum dots solar cells based on Graphene-TiO2 nanocomposite photoanode, Results Phys. 18 (2020), 103253.
[17] S. Abdallah, N. Al-Hosiny, A. Badawi, Photoacoustic study of CdS QDs for application in quantum-dot-sensitized solar cells, J. Nanomater. 2012 (2012).
[18] P. Roy, S.K. Srivastava, A new approach towards the growth of cadmium sulphide thin film by CBD method and its characterization, Mater. Chem. Phys. 95 (2–3) (2006) 235–241.
[19] D. Petre, et al., The influence of Cu doping on opto-electronic properties of chemically deposited CdS, Mater. Sci. Eng., B 58 (3) (1999) 238–243.
[20] R. Jayakrishnan, S. Kumar, R. Pandey, Rapid thermal annealing of multiple dip-coated CdS films, Semicond. Sci. Technol. 9 (1) (1994) 97.
[21] J.-H. Lee, et al., Electrical and optical properties of boron doped CdS thin films prepared by chemical bath deposition, Thin Solid Films 431 (2003) 344–348.
[22] P. Sebastian, p-type CdS thin films formed by in situ Cu doping in the chemical bath, Appl. Phys. Lett. 62 (23) (1993) 2956–2958.
[23] N. Megahid, et al., Microstructure and electrical conductivity of In-doped CdS thin films, Phys. B Condens. Matter 353 (3–4) (2004) 150–163.
[24] P. Roy, S.K. Srivastava, In situ deposition of Sn-doped CdS thin films by chemical bath deposition and their characterization, J. Phys. Appl. Phys. 39 (22) (2006) 4771.
[25] M. Khan, et al., Structural, electrical and optical properties of multilayer TiO2 thin films deposited by sol–gel spin coating, Results Phys. 7 (2017) 1437–1439.
[26] A. Khan, et al., Effect of Gd doping on structural, optical properties, photoluminescence and electrical characteristics of CdS nanoparticles for optoelectronics, Ceram. Int. 45 (8) (2019) 10133–10141.
[27] N. Venkatesh, et al., Visible light–driven photocatalytic dye degradation under natural sunlight using Sn-doped CdS nanoparticles, Environ. Sci. Pollut. Control Ser. 27 (34) (2020) 43212–43222.
[28] I. Yahia, et al., Chemically deposited Ni-doped CdS nanostructured thin films: optical analysis and current-voltage characteristics, J. Alloys Compd. 776 (2019) 1056–1062.
[29] A. Ibraheam, Y. Al-Douri, A. Azman, Characterization and analysis of wheat-like CdS nanostructures under temperature effect for solar cells applications, Optik 127 (20) (2016) 8907–8915.
[30] Z. Khan, et al., Improved photodetection performance of nanostructured CdS films based photodetectors via novel Er doping, J. Inorg. Organomet. Polym. Mater. 31 (9) (2021) 3880–3893.
[31] S. Singh, et al., Encompassing environment synthesis, characterization and photovoltaic utilization of cadmium sulphide quantum dots, Mater. Today Proc. 34 (2021) 767–770.
[32] F.K. Kharabaneh, et al., Rational design of chemical bath deposition technique for successful preparation of Mn-doped CdS nanostructured thin films with controlled optical properties, Ceram. Int. 47 (4) (2021) 5523–5533.
[33] A. Bahadur, M. Mishra, Correlation between refractive index and electronegativity difference for ANB8-N type binary semiconductors, Acta Phys. Pol., A 123 (4) (2013) 737–740.
[34] T.S. Moss, Photoconductivity in the elements, Proc. Phys. Soc. 64 (6) (1951) 590.
[35] P. Herve, L. Vandamme, General relation between refractive index and energy gap in semiconductors, Infrared Phys. Technol. 35 (4) (1994) 609–615.
[36] Daniel-Umeri, R.A., Effect of pH on the Optical Properties of Cadmium Sulphide (CdS) Thin Film Deposited Using Chemical Bath Method.
[37] N. Ravindra, S. Auluck, V. Srivastava, On the Penn gap in semiconductors, Phys. Status Solidi 93 (2) (1979) K155–K160.
[38] C. Aydin, Synthesis of Pd: ZnO nanofibers and their optical characterization dependent on modified morphological properties, J. Alloys Compd. 777 (2019) 145–151.
[39] B. Mehmood, et al., Structural and optical properties of Ti and Cu co-doped ZnO thin films for photovoltaic applications of dye sensitized solar cells, Int. J. Energy Res. 45 (2) (2021) 2445–2459.
[40] H.A. Hussin, Effect of fluorine doping on the optical properties of NiO thin films deposited by spray pyrolysis, IJSRSET Print Themed Section : Sci. Technol. 6 (4) (2019) 1–10.
[41] M. Kahouli, et al., Structural and optical properties of ZnO nanoparticles prepared by direct precipitation method, Superlattice. Microst. 85 (2015) 7–23.
[42] M. Akram, et al., CNTs mediated electrochemical performance and dielectric dispersion of TiO2-based hydrothermally synthesized nanocomposites, Ionics 27 (5) (2021) 2107–2118.
[43] A. Raza, et al., Morphology and dielectric studies of natural fibers and PbO2 based flexible composite sheets for potential energy storage applications, J. Electron. Mater. 49 (3) (2020) 1896–1903.
[44] A. Khalid, et al., Structural and dielectric properties of sol–gel synthesized (Mn, Cu) co-doped BiFeO3 ceramics, J. Sol. Gel Sci. Technol. 80 (3) (2016) 814–820.
[45] H. Rajbongshi, D. Kalita, Morphology-dependent photocatalytic degradation of organic pollutant and antibacterial activity with CdS nanostructures, J. Nanosci. Nanotechnol. 20 (9) (2020) 5885–5895.
[46] H. Moualkia, et al., Influence of the film thickness on the photovoltaic properties of chemically deposited CdS thin films: application to the photodegradation of orange II, Mater. Sci. Semicond. Process. 21 (2014) 186–193.
[47] M. Khan, et al., Effect of silver (Ag) ions irradiation on the structural, optical and photovoltaic properties of Mn doped TiO2 thin films based dye sensitized solar cells, Ceram. Int. 47 (11) (2021) 15801–15806.
[48] M. Khan, et al., Synthesis and characterization of Co and Ga co-doped ZnO thin films as an electrode for dye sensitized solar cells, Ceram. Int. 46 (17) (2020) 26590–26597.
[49] S. Hussain, et al., Decorating wide band gap CH3NH3PbBr3 perovskite with 4AMP for highly efficient and enhanced open circuit voltage perovskite solar cells, Sol. Energy 230 (2021) 501–508.
[50] M. Khan, et al., 900 keV Au ions implantation effect on the efficiency of dye sensitized solar cells, Results Phys. 14 (2019), 102425.
[51] J.H. Yang, et al., Characteristics of the dye-sensitized solar cells using TiO2 nanotubes treated with TiCl4, Materials 7 (5) (2014) 3522–3532.
[52] Z. Xiang, et al., Improving energy conversion efficiency of dye-sensitized solar cells by modifying TiO2 photoanodes with nitrogen-reduced graphene oxide, ACS Sustain. Chem. Eng. 2 (5) (2014) 1234–1240.
[53] A.S. Gonçalves, et al., Ga-modified nanostructured ZnO: characterization and application in dye-sensitized solar cells, in: Materials Science Forum, Trans Tech Publ, 2008.
[54] G. Kanimozhi, et al., A novel electrospun cobalt-doped zinc oxide nanofibers as photoanode for dye-sensitized solar cell, Mater. Res. Express 6 (2) (2018), 025041.